


Asperity-Level Origins of Transition from Mild to Severe Wear

Ramin Aghababaei,^{1,*} Tobias Brink,² and Jean-François Molinari²

¹Engineering Department, Aarhus University, 8000 Aarhus C, Denmark

²Civil Engineering Institute, École Polytechnique Fédérale de Lausanne (EPFL), Station 18, CH 1015 Lausanne, Switzerland
and Institute of Materials Science and Engineering, École Polytechnique Fédérale de Lausanne (EPFL),
Station 18, CH 1015 Lausanne, Switzerland

 (Received 29 August 2017; revised manuscript received 16 February 2018; published 4 May 2018)

Wear is the inevitable damage process of surfaces during sliding contact. According to the well-known Archard's wear law, the wear volume scales with the real contact area and as a result is proportional to the load. Decades of wear experiments, however, show that this relation only holds up to a certain load limit, above which the linearity is broken and a transition from mild to severe wear occurs. We investigate the microscopic origins of this breakdown and the corresponding wear transition at the asperity level. Our atomistic simulations reveal that the interaction between subsurface stress fields of neighboring contact spots promotes the transition from mild to severe wear. The results show that this interaction triggers the deep propagation of subsurface cracks and the eventual formation of large debris particles, with a size corresponding to the apparent contact area of neighboring contact spots. This observation explains the breakdown of the linear relation between the wear volume and the normal load in the severe wear regime. This new understanding highlights the critical importance of studying contact beyond the elastic limit and single-asperity models.

DOI: [10.1103/PhysRevLett.120.186105](https://doi.org/10.1103/PhysRevLett.120.186105)

Introduction.—The oldest and yet most fundamental wear relation states that the amount of material lost from a surface during sliding contact (i.e., wear volume) is proportional to the normal force applied to the surface [1–4]. This empirical observation is commonly rationalized by arguing that the wear process is a direct result of interactions among elevated surface asperities and therefore the wear volume scales with the real contact area, that is proportional to the normal load [5]. This linear relation, however, is only maintained within a certain range of applied loads [6], and breakdowns have been reported for lower [7,8] and higher [9–12] load limits. Therefore, the wear process is typically classified into the low, mild, and severe wear regimes, as summarized in Table I [9,13–18] and Fig. 1(a).

Inspired by this classification, we hypothesized different material removal mechanisms at the asperity level, which are schematically depicted in Figs. 1(b)–1(e). In the low

wear regime, surface asperities deform dominantly elasto-plastically and without significant formation of debris particles, as depicted in Fig. 1(c). In the mild wear regime, on the other hand, a fraction of the contacting surface asperities are detached by microcracking, resulting in tiny wear particles [Fig. 1(d)]. Inspired by the seminal work of Rabinowicz on the minimum size of debris particles [20], we found in a recent study that adhesive junctions below a critical size do not detach but smooth out plastically [21]. The transition from low to mild wear is thus connected to the growing junction sizes with increasing load. The experimentally observed linear relation between load and wear volume in the mild wear regime results from the fact that the volume of debris particles is proportional to the junction size [19,22].

Figure 1(e) illustrates a hypothesized asperity-level mechanism for severe wear: large subsurface cracks occur,

TABLE I. Wear regimes and mechanisms [9,13–18].

Wear regime	Wear mechanism	Wear debris	Wear coefficient	Wear volume vs load	Friction coefficient
Low wear	Localized surface deformation and plowing mechanisms	No observable debris	10^{-8} – 10^{-6}	Sublinear	$\mu < 0.01$
Mild wear	Surface microcracking and localized fracture at the asperity level	Tiny powderlike debris	10^{-4} – 10^{-2}	Linear	$0.01 < \mu < 0.5$
Severe wear	Subsurface crack propagation and macroscopic fracture	Large flakelike debris	10^{-2} –1	Superlinear	$\mu > 0.5$

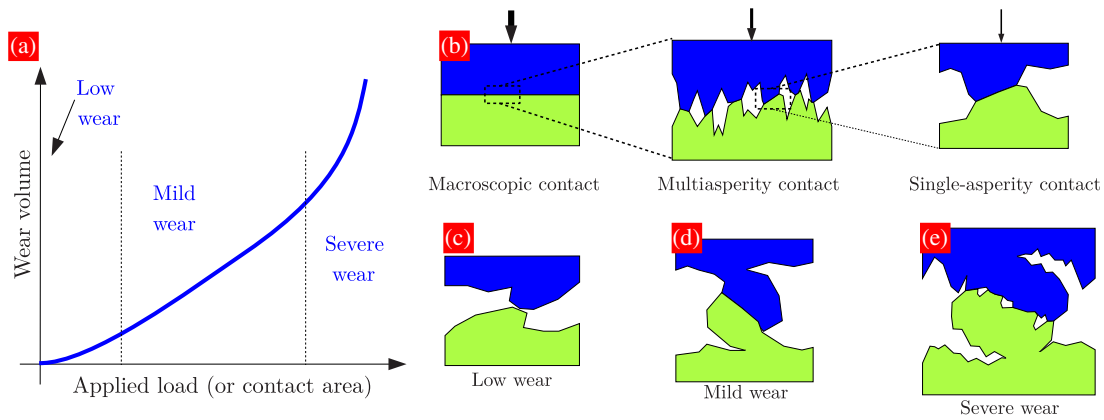


FIG. 1. Wear regimes and hypothesized asperity-level mechanisms. (a) A typical relation between wear volume and applied load in different wear regimes [9,13–18]. (b) The behavior of the macroscopically “flat” contact must be understood in terms of microscopic multi- and single-asperity contacts. (c) In the low wear regime, asperities are deformed elastoplastically without debris formation. (d) In the mild wear regime, elevated surface asperities are detached in the form of tiny debris particles. In this condition, the debris size is comparable to the junction size [19]. (e) In the severe wear regime, the formation of large wear debris particles occurs by deep crack propagation underneath the surface contact. The debris size then corresponds to the apparent contact area at the multiasperity level.

eventually leading to the formation of debris particles with sizes corresponding to that of the apparent contact area. As a result, the linear relation between the wear volume and normal load is violated, which is the key indicator of severe wear in macroscopic wear experiments [6,9]. While several engineering models have been developed for predicting the transition from mild to severe wear regimes [10,15,23], their predictions still rely on empirical data, as underlying transition mechanisms remain unclear. Considering the complex multiscale nature of the contact between sliding bodies [24–26], wear experiments [7,8,27–30] and numerical simulations [31–40] over the past decade have been focused on the investigation of wear processes at the single-asperity level.

Here, we present atomistic simulations that treat the transition from mild to severe wear as a multiasperity phenomenon. Our simulations reveal that this transition is governed by shielding interactions between subsurface cracks. As a result, debris particles with sizes corresponding to the apparent contact area instead of the real contact area are formed and the linear relation between wear volume and normal force is violated.

Method.—All simulations are molecular dynamics simulations performed in 2D and 3D with LAMMPS [41] using modified, nearest-neighbor Morse potentials [42]. The tail of these potentials is modified to embrittle the material and to be able to observe debris formation at computationally feasible length scales [21]. The 2D potential is P6 from Ref. [21] and the 3D potential is from Ref. [19]. Some details of the potentials and physical properties [43] are additionally recalled in the Supplemental Material [44]. We consider a strong interfacial adhesion between the two sliding bodies; i.e., the same interatomic potential is used for both the bulk and interface. The setup is similar as in Ref. [21], i.e., sliding simulations with a constant per atom normal load $0.001\epsilon/r_0$ and constant tangential velocity

$0.01r_0/t_0$ (t_0 is the reduced time unit) on a fixed layer on the top; see Supplemental Material Fig. S2 for a schematic [44]. We consider systems with two pairs of colliding asperities (semicircular or hemispherical). Periodic boundary conditions are applied in the sliding direction. This idealized setup allows well-defined parametric studies that are impossible with more realistic surface geometries, while retaining the essential physics of the process. Throughout the Letter, D and λ represent the asperity diameter and interspacing. Reduced units of ground-state bond length r_0 and bond energy ϵ are used. A Verlet algorithm with a time step $0.0025t_0$ is used for numerical integration. Langevin thermostats (with a damping parameter $0.05t_0$) at the boundaries were set to a temperature of $0.1\epsilon/k_B$. Analysis and visualization is conducted with OVITO [45], dislocations in 3D are detected with the dislocation extraction algorithm [46].

Results.—Since severe wear violates the relation between load and wear volume, we hypothesize that the reduced spacing between junctions at high load may promote subsurface interactions between those distinct junctions [47–49], which leads to a combined, multiasperity wear mechanism. To examine this hypothesis, we first consider a far-spaced pair of identical contacting asperities in 2D and 3D [Figs. 2(a) and 2(c)]. As expected, the collisions between surface asperities result in the formation of two isolated debris particles. Figure 2(b) presents the subsurface shear stress (that is vertically averaged over a subsurface layer with a thickness of the asperity diameter). It shows that the junctions are individually loaded to bulk shear strength τ_0 , where a weak subsurface interaction occurs. The loading ultimately leads to the nucleation of subsurface cracks and debris formation. In 3D, two isolated dislocation networks form in the areas of stress concentration [Fig. 2(d)], but otherwise the behavior is the same.

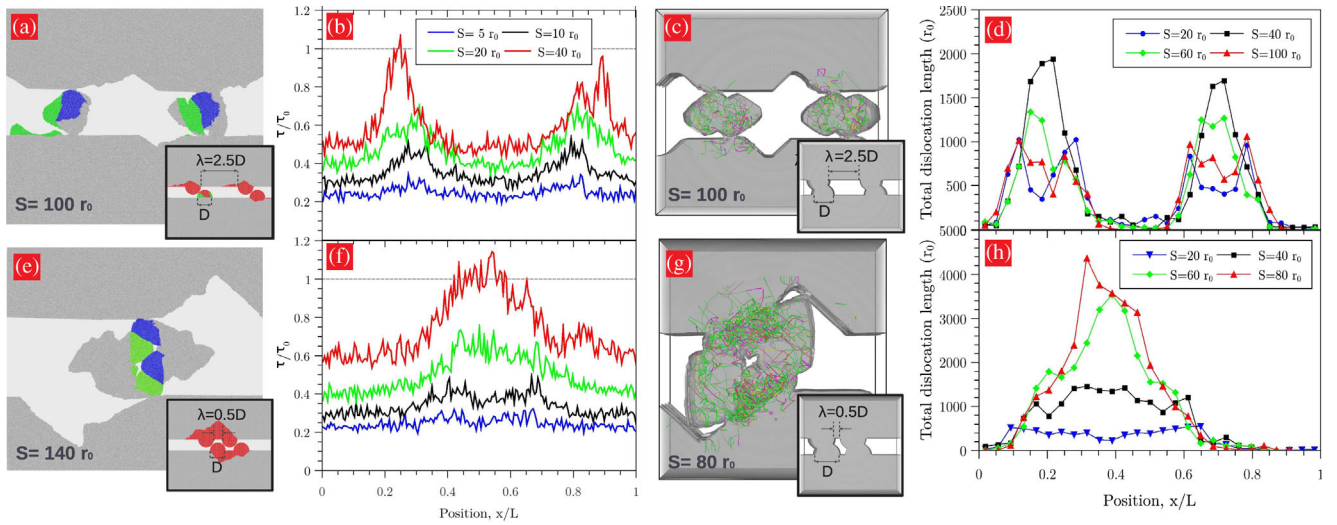


FIG. 2. Asperity-level wear mechanisms. Snapshots of debris formation in 2D (a), (e) and 3D (c), (g). The insets show the initial setup with $D = 60r_0$ (2D) and $D = 70r_0$ (3D). The total box length is $L = 7D$. The final detached volume (i.e., the debris atoms) is highlighted in red. Panels (b) and (f) show the subsurface shear stress vertically averaged over a subsurface layer with thickness D . Panels (d) and (h) depict the total dislocation length per bin size of $L/30$ for the 3D simulations.

A reduced spacing λ between the junctions, though, results in a different mechanism [Figs. 2(e) and 2(g)]: The junction pair jointly forms a single, big debris particle. While the junctions are loaded individually at the very onset of contact [Fig. 2(f)], their subsurface stress fields merge with increasing sliding distance S . In this situation, the proportionality between the junction and debris sizes is violated, as the debris size is associated with the apparent contact area between the two asperity junctions. This observation rationalizes the breakdown of the linear linear relation between the wear volume and the normal load (i.e., Archard’s wear law) in the severe wear regime.

This merging can be understood by considering that the formation of a particle is nothing but the development of a

crack that leads to its detachment [21]. Figure 3 presents a detailed analysis of the evolution of the stress component σ_{45° , which is perpendicular to the crack tips and therefore drives their nucleation and propagation. At the onset of sliding, identical stress concentrations develop at the base of both the leading and the trailing asperities [Fig. 3(a)], where subsurface cracks, marked as “inner” and “outer,” are nucleated [Fig. 3(b)]. With further sliding, however, the outer crack goes much deeper into the bulk as a consequence of the modified subsurface stress state. It can be seen that there is an asymmetry in that only the inner crack is unloaded. This is an effect of the somewhat peculiar loading conditions: The stress in the leading asperity (on the right in our setup) cannot be relieved by detaching the

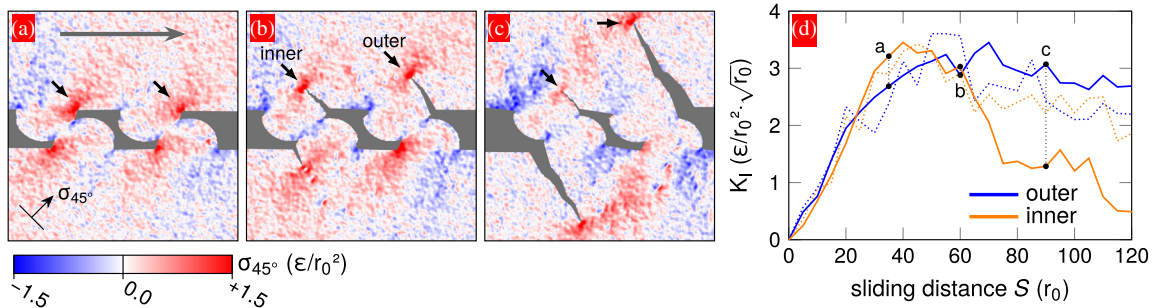


FIG. 3. Crack shielding drives joint debris formation. (a)–(c) Map of the stress component σ_{45° perpendicular to the crack tips, which drives the nucleation and propagation of the subsurface cracks. Simulation with $D = 100r_0$ and $\lambda = 0.7D$. The gray arrow indicates the sliding direction. At the onset of sliding (a), (b), the stress is concentrated identically at the corner of both asperities where subsurface cracks, marked as “inner” and “outer,” are nucleated. After further sliding, however, the inner crack is shielded by the outer one and closed (c), eventually resulting in joint debris formation. Panel (d) quantitatively supports this observation by showing a quick drop in the stress intensity factor of the inner crack. For comparison, data of a simulation with $\lambda = 2D$ are shown with dotted lines. No shielding occurs, both cracks grow, and two individual debris particles form. To minimize the thermal noise, both simulations were performed at a lower temperature $T = 0.045\epsilon/k_B$.

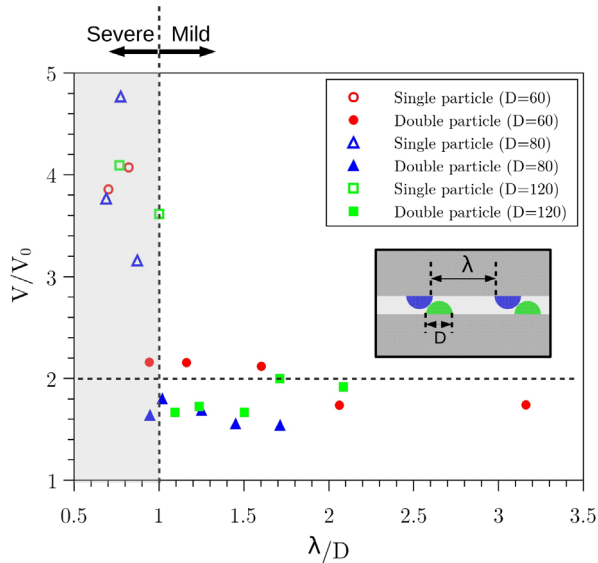


FIG. 4. Wear mechanisms and corresponding debris volume as a function of junction interspacing. (a) The cumulative wear volume is measured for simulations with similar loading and interfacial adhesion but different spacing λ between colliding pairs of asperities, for three initial asperity sizes D . The debris volume is normalized by a reference volume $V_0 = 2(\pi D^2/4)$, considering that each asperity is detached in the form of an idealized circular particle of the same diameter. Once $\lambda \leq D$, the debris volume exceeds this prediction and a transition from mild to severe wear occurs. In the severe wear regime (open symbols), the proportionality between the debris size and real contact area is violated.

trailing asperity, but a large outer crack can unload the trailing asperity. This observation offers a mechanism for the transition from mild to severe wear regimes at the asperity level: Depending on the interfacial adhesion and surface topography, neighboring microjunctions strongly interact through their subsurface stress fields, resulting in deep propagation of cracks into the bulk and the detachment of large debris particles.

The interaction between the subsurface cracks can also be quantified by the estimated stress intensity factor K_I of both cracks. For a detailed analysis of the stress intensity factor, a per-atom stress tensor is directly derived from the potential by LAMMPS and averaged over a radius of $3r_0$ to smooth out the noise by thermal fluctuations. The stress intensity factor K_I is estimated using the local stress field of σ_{45° around the stress tip. Since $\sigma = K_I f(\theta)/\sqrt{2\pi r}$ with $f(\theta) = \cos(\theta/2)[1 + \sin(\theta/2)\sin(3\theta/2)]$ [50], we calculate $\sigma/f(\theta)$ for each atom and fit the function $K_I/\sqrt{2\pi r}$ to this data (for $r < 25r_0$ and only for atoms with $-0.75\pi < \theta < 0.75\pi$ for numerical stability). Figure 3(d) shows that while both crack nucleation sites are initially loaded to the critical stress intensity factor K_{IC} , the inner crack is subsequently unloaded below the critical value. The dashed lines are the result of a similar setup with far-spaced

asperities, in which no unloading of the inner crack is observed.

This shielding effect is known for two parallel cracks subjected to mode I loading, which mutually reduce their stress intensity factor when their distance is smaller than 2–3 times their length (see also Supplemental Material Fig. S3 [44]) [51,52]. This argument explains why the joint debris formation only occurs with closely spaced junctions. Supplemental Material Fig. S4 [44] further supports this argument by showing that the shielding interaction can be suppressed by disconnecting the communication between the cracks. These observations also highlight the influence of subsurface inhomogeneities (e.g., grain boundaries, precipitates, and voids) on wear mechanisms.

Finally, we carried out a systematic set of simulations in 2D, each with different initial asperity size and spacing. Figure 4 summarizes the results by plotting the total debris volume versus the interspacing λ between colliding pairs of asperities for three different initial asperity sizes D . It can be seen that when $\lambda > D$, asperity junctions individually form two debris particles as shown in Fig. 2(a). However, once λ is comparable to D , a transition occurs and a single, large debris particle forms, as we expect from the discussion above. In addition, this is consistent with previous numerical [53] and analytical [47] studies that show that the contact solutions (i.e., the subsurface stress distribution and the displacement field) are remarkably different from those of the single asperity when the asperity spacing is comparable to the asperity diameter. One should note that the magnitude of this multiasperity length scale may be influenced by asperities geometries, subsurface microstructure, sliding distance, temperature, etc., which demand further systematic investigations in the future. Figure 4 also shows that the volume of single, large debris particles is significantly greater than the cumulative volume of two individually formed debris particles, confirming a larger material loss in the presence of asperity interactions. A detailed correlation between the wear volume and macroscopic components of load in the severe wear regime, however, requires further numerical and experimental studies.

Conclusion.—The key outcome of this study is the finding that closely spaced asperities are worn off together as a result of the interaction between subsurface stress fields, which can be explained in the context of fracture mechanics. This process leads to a wear volume proportional to the apparent contact area instead of the real contact area and thereby provides an asperity-level model for the transition from mild to severe wear. While this new understanding together with the critical junction size model [19,21] can be applied to simple multiasperity contact models [54,55] (i.e., two neighboring junctions jointly form a single big particle upon sliding if the spacing between them is smaller than their average size), it highlights a critical need for further fundamental studies in mechanics

and physics of contact [56–58]. We should note that, in this study, we have analyzed the interaction between idealized circular asperity junctions. Future studies should be dedicated to investigate the asperity junction interactions in more complex contact situations (e.g., lateral interaction perpendicular to the sliding direction, interaction between junctions with different sizes [59] and shapes [60], fractal rough contacts [22], etc.). Furthermore, the influence of surface roughness parameters, subsurface microstructure, and inhomogeneities such as precipitates or microcracks on the interaction length scale and surface cracking need to be yet investigated [35,61]. In summary, these results highlight a critical need for studying single- and multiasperity contact beyond the elastic limit [62–67].

The authors acknowledge financial support from the Swiss National Science Foundation (Grant No. 162569, “Contact mechanics of rough surfaces”). R. A. additionally acknowledges financial support from the Aarhus University Research Foundation, AUFR (Grant No. 27236, “Microscopic origins of adhesive wear”).

* aghababaei@eng.au.dk

- [1] E. Rabinowicz, *Friction and Wear of Materials* (Wiley, New York, 1995), pp. 125–166.
- [2] J. F. Archard, Contact and rubbing of flat surfaces, *J. Appl. Phys.* **24**, 981 (1953).
- [3] J. T. Burwell and C. D. Strang, On the empirical law of adhesive wear, *J. Appl. Phys.* **23**, 18 (1952).
- [4] R. Holm, in *Electrical Contacts*, edited by R. Holm (Springer, New York, 1946), pp. 232–242.
- [5] F. P. Bowden and D. Tabor, The area of contact between stationary and between moving surfaces, *Proc. R. Soc. A* **169**, 391 (1939).
- [6] J. F. Archard and W. Hirst, The wear of metals under unlubricated conditions, *Proc. R. Soc. A* **236**, 397 (1956).
- [7] T. D. B. Jacobs, B. Gotsmann, M. A. Lantz, and R. W. Carpick, On the application of transition state theory to atomic-scale wear, *Tribol. Lett.* **39**, 257 (2010).
- [8] B. Gotsmann and M. A. Lantz, Atomistic Wear in a Single Asperity Sliding Contact, *Phys. Rev. Lett.* **101**, 125501 (2008).
- [9] J. Zhang and A. Alpas, Transition between mild and severe wear in aluminium alloys, *Acta Mater.* **45**, 513 (1997).
- [10] K. Adachi, K. Kato, and N. Chen, Wear map of ceramics, *Wear* **203–204**, 291 (1997).
- [11] S. Hsu and M. Shen, Ceramic wear maps, *Wear* **200**, 154 (1996).
- [12] D. F. Wang and K. Kato, Nano-scale fatigue wear of carbon nitride coatings: Part I—Wear properties, *J. Tribol.* **125**, 430 (2003).
- [13] H. Kitsunai, K. Kato, K. Hokkirigawa, and H. Inoue, The transitions between microscopic wear modes during repeated sliding friction observed by a scanning electron microscope tribosystem, *Wear* **135**, 237 (1990).
- [14] K. Hokkirigawa, Wear mode map of ceramics, *Wear* **151**, 219 (1991).
- [15] Y. Wang and S. M. Hsu, Wear and wear transition modeling of ceramics, *Wear* **195**, 35 (1996).
- [16] S. Hsu and M. Shen, Wear prediction of ceramics, *Wear* **256**, 867 (2004).
- [17] K. Kato and K. Adachi, Wear of advanced ceramics, *Wear* **253**, 1097 (2002).
- [18] S. Wang, L. Wang, Y. Zhao, Y. Sun, and Z. Yang, Mild-to-severe wear transition and transition region of oxidative wear in steels, *Wear* **306**, 311 (2013).
- [19] R. Aghababaei, D. H. Warner, and J.-F. Molinari, On the debris-level origins of adhesive wear, *Proc. Natl. Acad. Sci. U.S.A.* **114**, 7935 (2017).
- [20] E. Rabinowicz, The effect of size on the looseness of wear fragments, *Wear* **2**, 4 (1958).
- [21] R. Aghababaei, D. H. Warner, and J.-F. Molinari, Critical length scale controls adhesive wear mechanisms, *Nat. Commun.* **7**, 11816 (2016).
- [22] L. Frérot, R. Aghababaei, and J.-F. Molinari, A mechanistic understanding of the wear coefficient: From single to multiple asperities contact, *J. Mech. Phys. Solids* **114**, 172 (2018).
- [23] S. Lim and M. Ashby, Overview no. 55 Wear-mechanism maps, *Acta Metall.* **35**, 1 (1987).
- [24] Y. Mo, K. T. Turner, and I. Szlufarska, Friction laws at the nanoscale, *Nature (London)* **457**, 1116 (2009).
- [25] B. Luan and M. O. Robbins, The breakdown of continuum models for mechanical contacts, *Nature (London)* **435**, 929 (2005).
- [26] C. Yang, U. Tartaglino, and B. N. Persson, A multiscale molecular dynamics approach to contact mechanics, *Eur. Phys. J. E* **19**, 47 (2006).
- [27] N. K. Sundaram, Y. Guo, and S. Chandrasekar, Mesoscale Folding, Instability, and Disruption of Laminar Flow in Metal Surfaces, *Phys. Rev. Lett.* **109**, 106001 (2012).
- [28] J. Liu, J. K. Notbohm, R. W. Carpick, and K. T. Turner, Method for characterizing nanoscale wear of atomic force microscope tips, *ACS Nano* **4**, 3763 (2010).
- [29] T. Sato, T. Ishida, L. Jalabert, and H. Fujita, Real-time transmission electron microscope observation of nanofriction at a single Ag asperity, *Nanotechnology* **23**, 505701 (2012).
- [30] A. Socoliuc, E. Gnecco, S. Maier, O. Pfeiffer, A. Baratoff, R. Bennewitz, and E. Meyer, Atomic-scale control of friction by actuation of nanometer-sized contacts, *Science* **313**, 207 (2006).
- [31] M. Ciavarella, On the effect of wear on asperity height distributions, and the corresponding effect in the mechanical response, *Tribol. Int.* **101**, 164 (2016).
- [32] X. Hu and A. Martini, Atomistic simulation of the effect of roughness on nanoscale wear, *Comput. Mater. Sci.* **102**, 208 (2015).
- [33] X. Hu, S. Sundararajan, and A. Martini, The effects of adhesive strength and load on material transfer in nanoscale wear, *Comput. Mater. Sci.* **95**, 464 (2014).
- [34] S. J. Eder, G. Feldbauer, D. Bianchi, U. Cihak-Bayr, G. Betz, and A. Vernes, Applicability of Macroscopic Wear and Friction Laws on the Atomic Length Scale, *Phys. Rev. Lett.* **115**, 025502 (2015).

- [35] A. Li and I. Szlufarska, How grain size controls friction and wear in nanocrystalline metals, *Phys. Rev. B* **92**, 075418 (2015).
- [36] Z.-D. Sha, V. Sorkin, P. S. Branicio, Q.-X. Pei, Y.-W. Zhang, and D. J. Srolovitz, Large-scale molecular dynamics simulations of wear in diamond-like carbon at the nanoscale, *Appl. Phys. Lett.* **103**, 073118 (2013).
- [37] G. Moras, L. Pastewka, P. Gumbsch, and M. Moseler, Formation and oxidation of linear carbon chains and their role in the wear of carbon materials, *Tribol. Lett.* **44**, 355 (2011).
- [38] L. Pastewka, S. Moser, P. Gumbsch, and M. Moseler, Anisotropic mechanical amorphization drives wear in diamond, *Nat. Mater.* **10**, 34 (2011).
- [39] V. L. Popov, Analytic solution for the limiting shape of profiles due to fretting wear, *Sci. Rep.* **4**, 3749 (2014).
- [40] H. Song, R. Dikken, L. Nicola, and E. Van der Giessen, Plastic ploughing of a sinusoidal asperity on a rough surface, *J. Appl. Mech.* **82**, 071006 (2015).
- [41] S. Plimpton, Fast parallel algorithms for short-range molecular dynamics, *J. Comput. Phys.* **117**, 1 (1995).
- [42] P. M. Morse, Diatomic molecules according to the wave mechanics. II. Vibrational levels, *Phys. Rev.* **34**, 57 (1929).
- [43] M. Ashby and D. Jones, *Engineering Materials* (Pergamon, Oxford, 1980).
- [44] See Supplemental Material at <http://link.aps.org/supplemental/10.1103/PhysRevLett.120.186105> for details of the used potentials and their physical properties, simulations geometry and boundary conditions. Further supporting results are also provided.
- [45] A. Stukowski, Visualization and analysis of atomistic simulation data with OVITO—The Open Visualization Tool, *Model. Simul. Mater. Sci. Eng.* **18**, 015012 (2010).
- [46] A. Stukowski, V. V. Bulatov, and A. Arsenlis, Automated identification and indexing of dislocations in crystal interfaces, *Model. Simul. Mater. Sci. Eng.* **20**, 085007 (2012).
- [47] C. Caroli and P. Nozières, Hysteresis and elastic interactions of microasperities in dry friction, *Eur. Phys. J. B* **4**, 233 (1998).
- [48] P. Nayak, Random process model of rough surfaces in plastic contact, *Wear* **26**, 305 (1973).
- [49] V. A. Yastrebov, J. Durand, H. Proudhon, and G. Cailletaud, Rough surface contact analysis by means of the finite element method and of a new reduced model, *C.R. Mec.* **339**, 473 (2011).
- [50] T. L. Anderson, *Fracture Mechanics: Fundamentals and Applications* (CRC Press, Boca Raton, FL, 2017).
- [51] *Stress Intensity Factors Handbook*, edited by Y. Murakami (Pergamon Press, New York, 1987).
- [52] W. A. Moussa, R. Bell, and C. L. Tan, The interaction of two parallel semi-elliptical surface cracks under tension and bending, *J. Pressure Vessel Technol.* **121**, 323 (1999).
- [53] K. Komvopoulos and D. Choi, Elastic finite element analysis of multi-asperity contacts, *J. Tribol.* **114**, 823 (1992).
- [54] J. A. Greenwood and B. P. Williamson, Contact of nominally flat surfaces, *Proc. R. Soc. Edinburgh, Sect. A* **295**, 300 (1966).
- [55] B. N. J. Persson and S. Gorb, The effect of surface roughness on the adhesion of elastic plates with application to biological systems, *J. Chem. Phys.* **119**, 11437 (2003).
- [56] V. Popov and G.-P. Ostermeyer, Numerical simulation methods in tribology: Possibilities and limitations, *Tribol. Int.* **40**, 915 (2007).
- [57] R. W. Carpick, The contact sport of rough surfaces, *Science* **359**, 38 (2018).
- [58] M. H. Müser *et al.*, Meeting the contact-mechanics challenge, *Tribol. Lett.* **65**, 118 (2017).
- [59] L. Pei, S. Hyun, J. Molinari, and M. O. Robbins, Finite element modeling of elasto-plastic contact between rough surfaces, *J. Mech. Phys. Solids* **53**, 2385 (2005).
- [60] V. L. Popov, R. Pohrt, and Q. Li, Strength of adhesive contacts: Influence of contact geometry and material gradients, Friction and wear in machinery **5**, 308 (2017).
- [61] Z. Farhat, Y. Ding, D. Northwood, and A. Alpas, Effect of grain size on friction and wear of nanocrystalline aluminum, *Mater. Sci. Eng. A* **206**, 302 (1996).
- [62] R. Aghababaei and S. P. Joshi, A crystal plasticity analysis of length-scale dependent internal stresses with image effects, *J. Mech. Phys. Solids* **60**, 2019 (2012).
- [63] H. Ghaednia, S. A. Pope, R. L. Jackson, and D. B. Marghitu, A comprehensive study of the elasto-plastic contact of a sphere and a flat, *Tribol. Int.* **93**, 78 (2016).
- [64] R. Jackson and I. Green, A finite element study of elasto-plastic hemispherical contact against a rigid flat, *J. Tribol.* **127**, 343 (2005).
- [65] F. Sun, E. V. der Giessen, and L. Nicola, Interaction between neighboring asperities during flattening: A discrete dislocation plasticity analysis, *Mech. Mater.* **90**, 157 (2015).
- [66] M. Ciavarella, V. Delfino, and V. Demelio, A new 2D asperity model with interaction for studying the contact of multiscale rough random profiles, *Wear* **261**, 556 (2006).
- [67] Y. Gao, C. J. Ruestes, D. R. Tramontina, and H. M. Urbassek, Comparative simulation study of the structure of the plastic zone produced by nanoindentation, *J. Mech. Phys. Solids* **75**, 58 (2015).